PHYSICAL REVIEW D **94,** 094020 (2016)

Light front quark-diquark model for the nucleons

Tanmay Maji and Dipankar Chakrabarti
Department of Physics, Indian Institute of Technology Kanpur, Kanpur 208016, India
(Received 19 September 2016; published 17 November 2016)

We present a quark-diquark model for the nucleons where the light front wave functions are constructed from the soft-wall AdS/QCD prediction. The model is consistent with the quark counting rule and Drell-Yan-West relation. The scale evolution of unpolarized parton distribution functions (PDFs) of protons is simulated by making the parameters in the PDF scale dependent. The evolution of the PDFs are reproduced for a wide range of evolution scale. Helicity and transversity distributions for the proton predicted in this model agree with phenomenological fits. The axial and tensor charges are also shown to agree with the experimental data. The model can be used to evaluate distributions like generalized parton distributions, transverse momentum dependent distributions, etc., and their scale evolutions.

DOI: 10.1103/PhysRevD.94.094020

I. INTRODUCTION

In recent years, there have been many activities investigating the three-dimensional structure of protons. Different model investigations have given many interesting insights into the nucleon structure and interrelations among different distribution functions like transverse momentum dependent distributions (TMDs), generalized parton distributions (GPDs), Wigner distributions, etc., and their properties. There have been many model calculations for integrated parton distribution functions (PDFs), but for TMDs and Wigner distributions, only a few such model calculations are available. Since different experiments produce data at different energy scales, predictions of the scale evolutions of these different distributions are also very important. In this paper, we build a simple but phenomenological quark-diquark model for the nucleons that can be used to calculate all these distributions and their interrelations, and at the same time we also evaluate the scale evolutions of different distributions.

The quark-diquark model describes a nucleon as a composite of a diquark spectator with a definite mass and an active quark. The model assumes the factorization of short-distance (hard) and long-distance (soft) dynamics in high energy scattering and assumes that the lepton basically scatters off a single quark in a nucleon; the other two quarks can be treated as a composite diquark spectator. The diquarks are the effective degrees of freedom and the nonperturbative gluon exchanges between the two spectator quarks are taken into account by considering an invariant mass of the diquark. This simple model of nucleons is very successful in describing many interesting phenomena. There are many different variations or parametrizations of the quark-diquark model in the literature [1–4]. Here we want to construct a quark-diquark model for protons with light front wave functions, which should not only include the valence structure but also some of its nonperturbative ingredients. Light front AdS/QCD provides one such choice. Light front AdS/QCD predicts a general form of two-particle bound state wave function that cannot be derived from valence quarks alone [5]. One needs an infinite number of Fock states to have that wave function and thus it includes nonperturbative information. Recently, the light front wave functions for the nucleons in quark-scalar-diquark models [6,7] have been constructed from the light front AdS/QCD prediction. These models have been applied to evaluate many interesting properties of protons, e.g., GPDs, Wigner distributions, TMDs etc. [8,9]. Recently, some interesting relations among the GPDs and TMDs have been investigated [10] in the scalar diquark model [6] with the light front wave functions modeled from a soft-wall AdS/QCD wave function. Though the models successfully describe many nucleon properties, they include only the scalar diquark state. In the quark model, the nucleons consist of three quarks of two different flavors u and d ($p = |uud\rangle, n = |udd\rangle$). In the quark-diquark picture, we can schematically write, for example, the proton state $p = |u(ud)\rangle + |d(uu)\rangle$, where (ud) and (uu) are the diquark states. With spin-flavor symmetry, the diquark can be either scalar or axial vector, and hence both of them are required to build a model. Scalar diquarks alone cannot give the complete picture of a nucleon.

In this work, we construct a quark-diquark model with $SU(4)$ spin-flavor structure for the nucleons with the light front wave functions modeled from the AdS/QCD prediction, including both the scalar and axial vector diquarks. The model is consistent with the quark counting rule and Drell-Yan-West relation. The parameters are fitted to proton form factors and unpolarized PDF data at the initial scale μ_0. We consider the leading order QCD evolution of the unpolarized PDF for the proton and set the initial scale to $\mu_0 = 0.313$ GeV [6,11]. The scale evolution of the PDFs are simulated by introducing scale dependence in the parameters. The model reproduces the PDF scale evolution up to a very high scale. The helicity distribution $g_1(x, \mu)$ and transversity distribution $h_1(x, \mu)$ are predicted in this model at different scales μ. We can also get numerical estimation of different physical quantities to match with the available data. We show that the predictions of tensor and

axial charges in this model are in good agreement with the observed data.

In Sec. II, we describe the quark-diquark model with detailed expressions of the light front wave functions. The parameters in the model are fitted to the proton form factors and the details are discussed in Sec. III. In Sec. IV, we discuss the scale evolution of the unpolarized PDFs. In Sec. V, we discuss the polarized PDFs and the axial and tensor charges predicted in our model. Finally, we present a brief summary and conclusion in Sec. VI.

II. DIQUARK MODEL

In the diquark model, we assume that the virtual incoming photon is interacting with a valence quark and two other valence quarks form a diquark of definite mass with spin 0, called a scalar diquark, or with spin 1, called a vector diquark. The spin-0 diquarks are in a flavor singlet state and spin-1 diquarks are in a flavor triplet state. The proton state is written as a sum of isoscalar-scalar diquark singlet state $|uS^0\rangle$, isoscalar-vector diquark state $|uA^0\rangle$, and isovector-vector diquark state $|dA^1\rangle$ [3,4]. The proton state is written in the spin-flavor $SU(4)$ structure as

$$|P;\pm\rangle = C_S|uS^0\rangle^{\pm} + C_V|uA^0\rangle^{\pm} + C_{VV}|dA^1\rangle^{\pm}, \quad (1)$$

where S and A represent the scalar and vector diquarks having isospin as their superscript. Under the isospin symmetry, the neutron state is given by the above formula with $u \leftrightarrow d$.

We use the light-cone convention $x^{\pm} = x^0 \pm x^3$. We choose a frame where the transverse momentum of protons vanishes, i.e., $P \equiv (P^+, \frac{M^2}{P^+}, \mathbf{0}_\perp)$, where the momentum of the struck quark is $p \equiv (xP^+, \frac{p^2+|\mathbf{p}_\perp|^2}{xP^+}, \mathbf{p}_\perp)$ and that of diquark is $P_X \equiv ((1-x)P^+, P_X^-, -\mathbf{p}_\perp)$. Here $x = p^+/P^+$ is the longitudinal momentum fraction carried by the struck quark. The two-particle Fock-state expansion for $J^z = \pm 1/2$ with the spin-0 diquark is given by

$$|uS\rangle^{\pm} = \int \frac{dxd^2\mathbf{p}_\perp}{2(2\pi)^3\sqrt{x(1-x)}}\left[\psi_+^{\pm(u)}(x,\mathbf{p}_\perp)|+\frac{1}{2};xP^+,\mathbf{p}_\perp\rangle + \psi_-^{\pm(u)}(x,\mathbf{p}_\perp)|-\frac{1}{2}s;xP^+,\mathbf{p}_\perp\rangle\right], \quad (2)$$

and the light-front wave functions (LFWFs) with spin-0 diquark, for $J = \pm 1/2$, are given by [12]

$$\begin{aligned}
\psi_+^{+(u)}(x,\mathbf{p}_\perp) &= N_S\varphi_1^{(u)}(x,\mathbf{p}_\perp),\\
\psi_-^{+(u)}(x,\mathbf{p}_\perp) &= N_S\left(-\frac{p^1+ip^2}{xM}\right)\varphi_2^{(u)}(x,\mathbf{p}_\perp)\\
\psi_+^{-(u)}(x,\mathbf{p}_\perp) &= N_S\left(\frac{p^1-ip^2}{xM}\right)\varphi_2^{(u)}(x,\mathbf{p}_\perp),\\
\psi_-^{-(u)}(x,\mathbf{p}_\perp) &= N_S\varphi_1^{(u)}(x,\mathbf{p}_\perp),
\end{aligned} \quad (3)$$

where $|\lambda_q\lambda_S;xP^+,\mathbf{p}_\perp\rangle$ is the two-particle state having a struck quark of helicity λ_q and a scalar diquark having helicity $\lambda_S = s$ (the spin-0 singlet diquark helicity is denoted by s to distinguish it from that of the triplet diquark). The state with a spin-1 diquark is given as [13]

$$\begin{aligned}
|\nu A\rangle^{\pm} = \int \frac{dxd^2\mathbf{p}_\perp}{2(2\pi)^3\sqrt{x(1-x)}}\Big[&\psi_{++}^{\pm(\nu)}(x,\mathbf{p}_\perp)|+\frac{1}{2}+1;xP^+,\mathbf{p}_\perp\rangle\\
&+\psi_{-+}^{\pm(\nu)}(x,\mathbf{p}_\perp)|-\frac{1}{2}+1;xP^+,\mathbf{p}_\perp\rangle+\psi_{+0}^{\pm(\nu)}(x,\mathbf{p}_\perp)|\\
&+\frac{1}{2}0;xP^+,\mathbf{p}_\perp\rangle+\psi_{-0}^{\pm(\nu)}(x,\mathbf{p}_\perp)|-\frac{1}{2}0;xP^+,\mathbf{p}_\perp\rangle\\
&+\psi_{+-}^{\pm(\nu)}(x,\mathbf{p}_\perp)|+\frac{1}{2}-1;xP^+,\mathbf{p}_\perp\rangle\\
&+\psi_{--}^{\pm(\nu)}(x,\mathbf{p}_\perp)|-\frac{1}{2}-1;xP^+,\mathbf{p}_\perp\rangle\Big],
\end{aligned} \quad (4)$$

where $|\lambda_q\lambda_D;xP^+,\mathbf{p}_\perp\rangle$ represents a two-particle state with a quark of helicity $\lambda_q = \pm\frac{1}{2}$ and a vector diquark of helicity $\lambda_D = \pm 1, 0(triplet)$. The LFWFs are, for $J = +1/2$,

$$\begin{aligned}
\psi_{++}^{+(\nu)}(x,\mathbf{p}_\perp) &= N_1^{(\nu)}\sqrt{\frac{2}{3}}\left(\frac{p^1-ip^2}{xM}\right)\varphi_2^{(\nu)}(x,\mathbf{p}_\perp),\\
\psi_{-+}^{+(\nu)}(x,\mathbf{p}_\perp) &= N_1^{(\nu)}\sqrt{\frac{2}{3}}\varphi_1^{(\nu)}(x,\mathbf{p}_\perp),\\
\psi_{+0}^{+(\nu)}(x,\mathbf{p}_\perp) &= -N_0^{(\nu)}\sqrt{\frac{1}{3}}\varphi_1^{(\nu)}(x,\mathbf{p}_\perp),\\
\psi_{-0}^{+(\nu)}(x,\mathbf{p}_\perp) &= N_0^{(\nu)}\sqrt{\frac{1}{3}}\left(\frac{p^1+ip^2}{xM}\right)\varphi_2^{(\nu)}(x,\mathbf{p}_\perp),\\
\psi_{+-}^{+(\nu)}(x,\mathbf{p}_\perp) &= 0,\\
\psi_{--}^{+(\nu)}(x,\mathbf{p}_\perp) &= 0,
\end{aligned} \quad (5)$$

and for $J = -1/2$,

$$\begin{aligned}
\psi_{++}^{-(\nu)}(x,\mathbf{p}_\perp) &= 0,\\
\psi_{-+}^{-(\nu)}(x,\mathbf{p}_\perp) &= 0,\\
\psi_{+0}^{-(\nu)}(x,\mathbf{p}_\perp) &= N_0^{(\nu)}\sqrt{\frac{1}{3}}\left(\frac{p^1-ip^2}{xM}\right)\varphi_2^{(\nu)}(x,\mathbf{p}_\perp),\\
\psi_{-0}^{-(\nu)}(x,\mathbf{p}_\perp) &= N_0^{(\nu)}\sqrt{\frac{1}{3}}\varphi_1^{(\nu)}(x,\mathbf{p}_\perp),\\
\psi_{+-}^{-(\nu)}(x,\mathbf{p}_\perp) &= -N_1^{(\nu)}\sqrt{\frac{2}{3}}\varphi_1^{(\nu)}(x,\mathbf{p}_\perp),\\
\psi_{--}^{-(\nu)}(x,\mathbf{p}_\perp) &= N_1^{(\nu)}\sqrt{\frac{2}{3}}\left(\frac{p^1+ip^2}{xM}\right)\varphi_2^{(\nu)}(x,\mathbf{p}_\perp),
\end{aligned} \quad (6)$$

having flavor index $\nu = u, d$. The LFWFs $\varphi_i^{(\nu)}(x,\mathbf{p}_\perp)$ are a modified form of the soft-wall AdS/QCD prediction [6]

$$\varphi_i^{(\nu)}(x,\mathbf{p}_\perp)=\frac{4\pi}{\kappa}\sqrt{\frac{\log(1/x)}{1-x}}x^{a_i^\nu}(1-x)^{b_i^\nu}\times\exp\left[-\delta^\nu\frac{\mathbf{p}_\perp^2}{2\kappa^2}\frac{\log(1/x)}{(1-x)^2}\right]. \quad (7)$$

The wave functions $\varphi_i^\nu(i=1,2)$ reduce to the AdS/QCD prediction [5] for the parameters $a_i^\nu=b_i^\nu=0$ and $\delta^\nu=1.0$. We use the AdS/QCD scale parameter $\kappa=0.4$ GeV as determined in [14] and the quarks are assumed to be massless.

III. FORM FACTOR FITTING

In the light front formalism, for a spin-$\frac{1}{2}$ composite particle system the Dirac and Pauli form factors are defined as [15]

$$\langle P+q;+|\frac{J^+(0)}{2P^+}|P;+\rangle=F_1(q^2) \quad (8)$$

$$\langle P+q;+|\frac{J^+(0)}{2P^+}|P;-\rangle=-(q^1-iq^2)\frac{F_2(q^2)}{2M}, \quad (9)$$

where q^2 is the square of the momentum transferred to the nucleon of mass M. The normalizations of form factors for protons and neutrons are given as $F_1^p(0)=1$, $F_2^p(0)=\kappa^p=1.793$, and $F_1^n(0)=0$, $F_2^n(0)=\kappa^n=-1.913$, respectively. Considering the charge and isospin symmetry, we can decompose the nucleon form factors into flavor form factors as [16] $F_i^{p(n)}=e_uF_i^{u(d)}+e_dF_i^{d(u)}$.

In the SU(4) structure, flavored form factors are written in terms of scalar and vector diquarks as [4]

$$F_i^{(u)}(Q^2)=C_S^2F_i^{(S)}(Q^2)+C_V^2F_i^{(V)}(Q^2), \quad (10)$$

$$F_i^{(d)}(Q^2)=C_{VV}^2F_i^{(VV)}(Q^2). \quad (11)$$

In the quark-diquark model, Dirac and Pauli form factors for quarks can be written in terms of LFWFs as

$$F_1^{(S)}(Q^2)=\int_0^1\int\frac{d^2\mathbf{p}_\perp}{16\pi^3}[\psi_+^{+(u)\dagger}(x,\mathbf{p}'_\perp)\psi_+^{+(u)}(x,\mathbf{p}_\perp)+\psi_-^{+(u)\dagger}(x,\mathbf{p}'_\perp)\psi_-^{+(u)}(x,\mathbf{p}_\perp)], \quad (12)$$

$$F_2^{(S)}(Q^2)=-\frac{2M}{q^1-iq^2}\int_0^1\int\frac{d^2\mathbf{p}_\perp}{16\pi^3}[\psi_+^{+(u)\dagger}(x,\mathbf{p}'_\perp)\psi_+^{-(u)}(x,\mathbf{p}_\perp)+\psi_-^{+(u)\dagger}(x,\mathbf{p}'_\perp)\psi_-^{-(u)}(x,\mathbf{p}_\perp)], \quad (13)$$

for the scalar diquark and

$$F_1^{(A)}(Q^2)=\int_0^1\int\frac{d^2\mathbf{p}_\perp}{16\pi^3}[\psi_{++}^{+(\nu)\dagger}(x,\mathbf{p}'_\perp)\psi_{++}^{+(\nu)}(x,\mathbf{p}_\perp)+\psi_{-+}^{+(\nu)\dagger}(x,\mathbf{p}'_\perp)\psi_{-+}^{+(\nu)}(x,\mathbf{p}_\perp)+\psi_{+0}^{+(\nu)\dagger}(x,\mathbf{p}'_\perp)\psi_{+0}^{+(\nu)}(x,\mathbf{p}_\perp)+\psi_{-0}^{+(\nu)\dagger}(x,\mathbf{p}'_\perp)\psi_{-0}^{+(\nu)}(x,\mathbf{p}_\perp)], \quad (14)$$

$$F_2^{(A)}(Q^2)=-\frac{2M}{q^1-iq^2}\int_0^1\int\frac{d^2\mathbf{p}_\perp}{16\pi^3}[\psi_{+0}^{+(\nu)\dagger}(x,\mathbf{p}'_\perp)\psi_{+0}^{-(\nu)}(x,\mathbf{p}_\perp)+\psi_{-0}^{+(\nu)\dagger}(x,\mathbf{p}'_\perp)\psi_{-0}^{-(\nu)}(x,\mathbf{p}_\perp)] \quad (15)$$

for the vector diquark, where $\mathbf{p}'_\perp=\mathbf{p}_\perp+(1-x)\mathbf{q}_\perp$. The superscript $A=V,VV$ for the isoscalar-vector diquark and isovector-vector diquark, respectively. We consider the frame where $q=(0,0,\mathbf{q}_\perp)$ and $Q^2=-q^2=\mathbf{q}_\perp^2$.

In this model, the Dirac and Pauli form factors read

$$F_1^{(S)}(Q^2)=N_S^2R_1^{(u)}(Q^2) \quad (16)$$

$$F_2^{(S)}(Q^2)=N_S^2R_2^{(u)}(Q^2) \quad (17)$$

$$F_1^{(V)}(Q^2)=\left(\frac{1}{3}N_0^{(u)2}+\frac{2}{3}N_1^{(u)2}\right)R_1^{(u)}(Q^2) \quad (18)$$

$$F_2^{(V)}(Q^2)=-\frac{1}{3}N_0^{(u)2}R_2^{(u)}(Q^2) \quad (19)$$

$$F_1^{(VV)}(Q^2)=\left(\frac{1}{3}N_0^{(d)2}+\frac{2}{3}N_1^{(d)2}\right)R_1^{(d)}(Q^2) \quad (20)$$

$$F_2^{(VV)}(Q^2)=-\frac{1}{3}N_0^{(d)2}R_2^{(d)}(Q^2), \quad (21)$$

where the superscripts S, V, and VV represent the contributions with isoscalar-scalar diquark, isoscalar-vector diquark, and isovector-vector diquarks, respectively. $R_1^{(\nu)}(Q^2)$ and $R_2^{(\nu)}(Q^2)$ are defined as

$$R_1^{(\nu)}(Q^2)=\int dx\left[T_1^{(\nu)}(x)\frac{(1-x)^2}{\delta^\nu}+T_2^{(\nu)}(x)\frac{(1-x)^4}{(\delta^\nu)^2}\frac{\kappa^2}{M^2\log(1/x)}\times\left(1-\frac{\delta^\nu Q^2}{4\kappa^2}\log(1/x)\right)\right]\exp\left[-\delta^\nu\frac{Q^2}{4\kappa^2}\log(1/x)\right], \quad (22)$$

$$R_2^{(\nu)}(Q^2)=\int dx2T_3^{(\nu)}(x)\frac{(1-x)^3}{\delta^\nu}\exp\left[-\delta^\nu\frac{Q^2}{4\kappa^2}\log(1/x)\right], \quad (23)$$

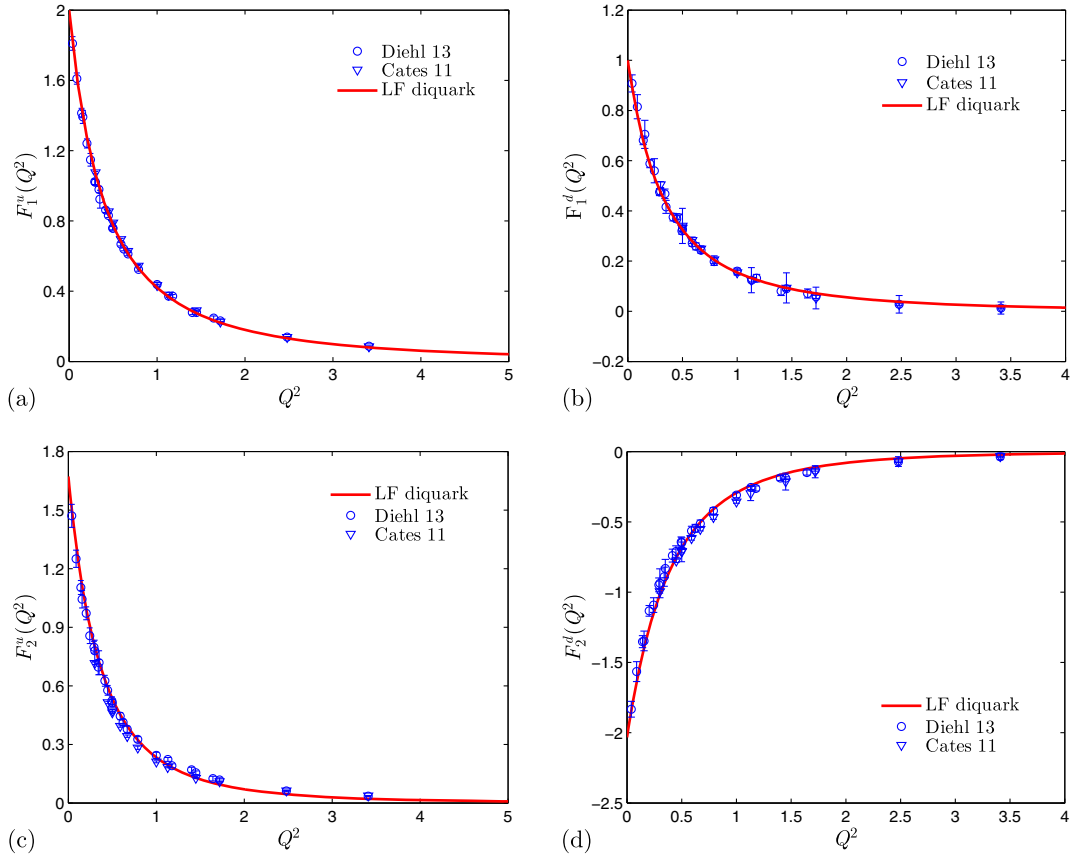

FIG. 1. Flavor form factors fitting in the light front diquark model. Data are taken from Refs. [16,17].

where

$$T_1^{(\nu)}(x) = x^{2a_1^\nu}(1-x)^{2b_1^\nu-1}, \tag{24}$$

$$T_2^{(\nu)}(x) = x^{2a_2^\mu-2}(1-x)^{2b_2^\nu-1}, \tag{25}$$

$$T_3^{(\nu)}(x) = x^{a_1^\nu+a_2^\nu-1}(1-x)^{b_1^\nu+b_2^\nu-1}. \tag{26}$$

We find the values of the parameters a_i and b_i by fitting the Dirac and Pauli form factors data taken form Refs. [16,17]. The parameters are listed in Table I. Figure 1 shows the form factor fittings in our model.

The normalization conditions are defined as

$$\int_0^1 dx f_1^{(u)}(x) = F_1^{(u)}(Q^2=0) = n_u, \tag{27}$$

$$\int_0^1 dx E_1^{(u)}(x,0) = F_2^{(u)}(Q^2=0) = \kappa_u, \tag{28}$$

$$\int_0^1 dx f_1^{(d)}(x) = F_1^{(d)}(Q^2=0) = n_d, \tag{29}$$

$$\int_0^1 dx E_1^{(d)}(x,0) = F_2^{(d)}(Q^2=0) = \kappa_d, \tag{30}$$

where $f_1^\nu(x)$ is the unpolarized PDF and $E^{(\nu)}(x,Q^2)$ is the helicity flip GPD corresponding to the valence quark of flavor $\nu = u$, d, and according to the quark counting rules $n_u = 2$ and $n_d = 1$ for protons. From isospin symmetry, the anomalous magnetic moments for u and d quarks are $\kappa_u = 1.673$ and $\kappa_d = -2.033$, respectively. The coefficients C_i^2 are then determined as

$$\begin{aligned} C_S^2 &= 1.3872, \\ C_V^2 &= 0.6128, \\ C_{VV}^2 &= 1. \end{aligned} \tag{31}$$

The flavor decomposition of any distribution function follows the Eqs. (10)–(11), with C_i^2 given above in Eq. (31).

The normalized constants N_i^2 are found considering the following normalizations [4]:

$$\int dx f_1^{(S)}(x) = F_1^{(S)}(0) = 1, \quad \int dx f_1^{(V)}(x) = F_1^{(V)}(0) = 1,$$
$$\int dx f_1^{(VV)}(x) = F_1^{(VV)}(0) = 1;$$

and the values are $N_S = 2.0191$, $N_0^{(u)} = 3.2050$, $N_0^{(d)} = 5.9423$, $N_1^{(u)} = 0.9895$, $N_1^{(d)} = 1.1616$. To demonstrate the accuracy of the model, in Fig. 2, the flavor form factors multiplied with Q^2 are compared with the available data. Even at large Q^2, the model predictions are within error bars of the experimental data.

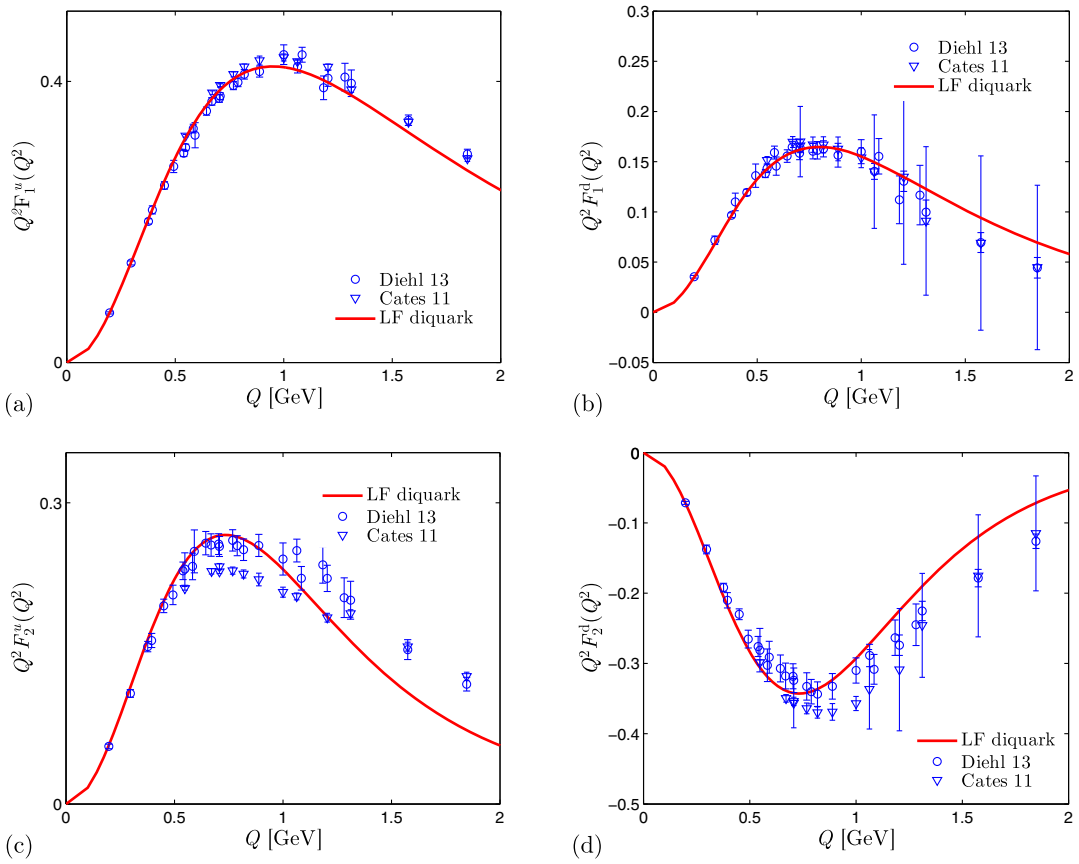

FIG. 2. Dirac and Pauli form factors multiplied by Q^2 for u and d quarks and compared with the data [16,17].

The Sachs form factors for nucleons ($i = p,\ n$) are defined as

$$G_E^i(Q^2) = F_1^i(Q^2) - \frac{Q^2}{4M_i^2}F_2^i(Q^2), \tag{32}$$

$$G_M^i(Q^2) = F_1^i(Q^2) + F_2^i(Q^2). \tag{33}$$

In Fig. 3, the Sachs form factors G_E and G_M for protons and neutrons in this model are shown to have excellent agreement with the experimental data, except for G_M^n. The ratios $R^i = \mu_i G_E^i/G_M^i$ for protons and neutrons are also shown in Fig. 4. They agree with the experimental data quite well. In Fig. 4(a), our results agree with the experimental data obtained in the Rosenbluth method, which involve one-photon exchange, while at large Q^2, they deviate from the data [18] from the polarization transfer method, which involves two-photon exchange. We also calculate the electromagnetic radii of nucleons from

$$\langle r_E^2\rangle^i = -6\frac{dG_E^i(q^2)}{dQ^2}\bigg|_{Q^2=0}, \tag{34}$$

$$\langle r_M^2\rangle^i = -\frac{6}{G_M^i(0)}\frac{dG_M^i(q^2)}{dQ^2}\bigg|_{Q^2=0}, \tag{35}$$

in this model. The radii given in Table II show quite good agreement with measured data. The proton charge radius r_E^p in our model is in better agreement with the muonic hydrogen data $r_E^p = 0.84087(39)$ fm [19].

IV. UNPOLARIZED PDF EVOLUTION

The parton distribution function is defined as

$$\Phi^{\Gamma(\nu)}(x) = \frac{1}{2}\int\frac{dz^-}{2(2\pi)}e^{ip^+z^-/2} \times \langle P;S|\bar\psi^{(\nu)}(0)\Gamma\psi^{(\nu)}(z^-)|P;S\rangle|_{z^+=z_T=0}, \tag{36}$$

which depends only on the light-cone momentum fraction $x = p^+/P^+$. The proton state $|P;S\rangle$, having spin S, is given in Eq. (1). For different Dirac structures we get different PDFs, e.g., for $\Gamma = \gamma^+, \gamma^+\gamma^5, i\sigma^{j+}\gamma^5$ we have the unpolarized PDF $f_1(x)$, helicity distribution $g_1(x)$, and transversity distribution $h_1(x)$, respectively.

The leading order QCD evolution of the unpolarized PDF is given as [11]

$$\int_0^1 dx x^n f_1(x,\mu) = \left(\frac{\alpha_s(\mu)}{\alpha_s(\mu_0)}\right)^{\gamma_n^{(0)}/2\beta_0}\int_0^1 dx x^n f_1(x,\mu_0), \tag{37}$$

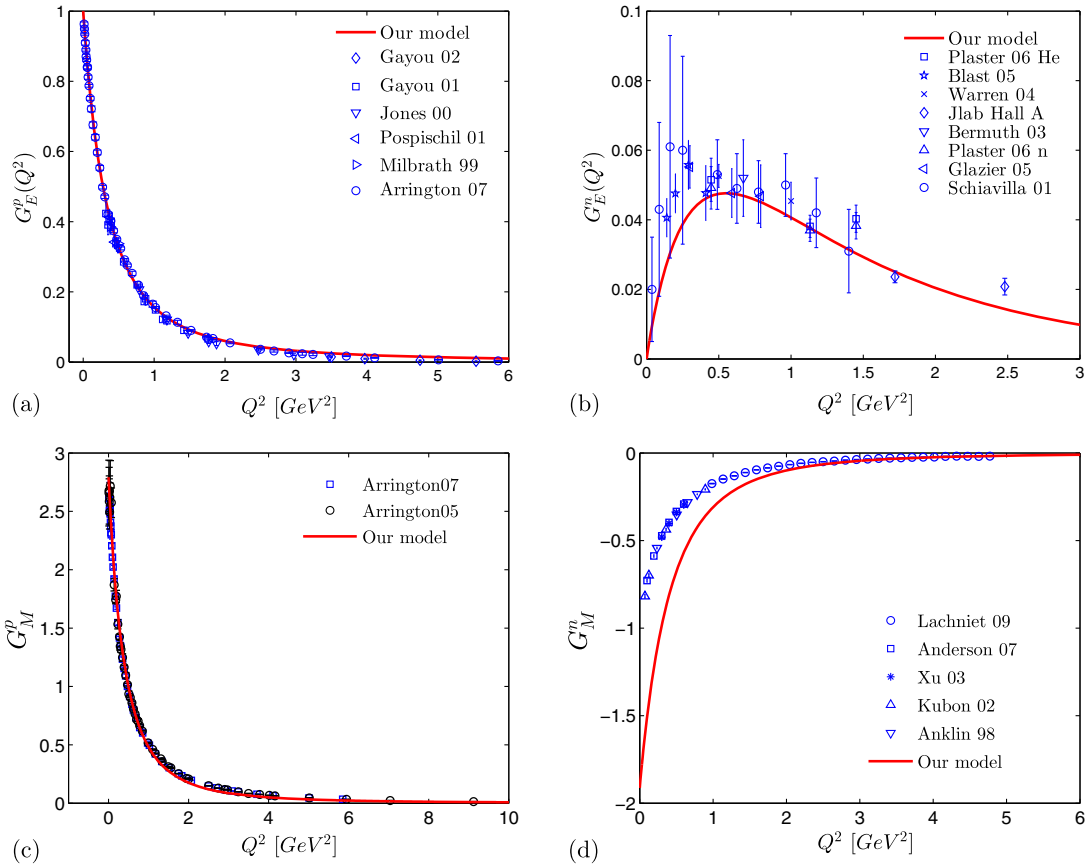

FIG. 3. Sachs form factors $G_E^{p(n)}(Q^2)$ and $G_M^{p(n)}(Q^2)$ for protons [(a) and (c)] and neutrons [(b) and (d)], respectively. The data are taken from Refs. [20–25] for $G_E^p(Q^2)$, Refs. [26–32] for $G_E^n(Q^2)$, Refs. [22,33] for $G_M^p(Q^2)$, and Refs. [34–38] for $G_M^n(Q^2)$.

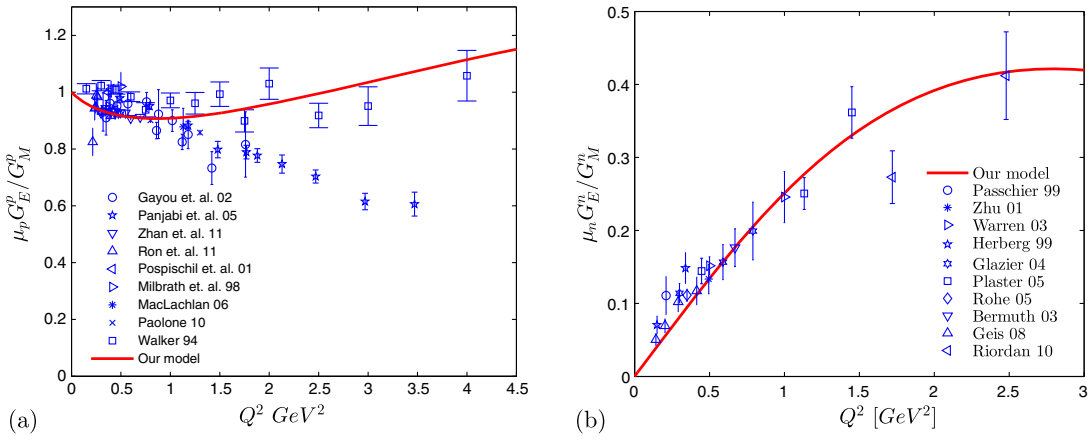

FIG. 4. Ratio of Sachs form factor $R^i = \mu_i G_E^i/G_M^i$ for protons [18,23–25,39–43] and neutrons [26,27,29–31,44–47].

where the anomalous dimension is given as

$$\gamma_n^{(0)} = -2C_F\left(3 + \frac{2}{(n+1)(n+2)} - 4\sum_{k=1}^{n+1}\frac{1}{k}\right), \quad (38)$$

with $C_F = 4/3$ and $\beta_0 = 9$. The strong coupling constant, at the leading order, is given as

$$\alpha_s(\mu) = \frac{4\pi}{\beta_0 \ln(\mu^2/\Lambda_{\rm QCD}^2)} \quad (39)$$

with $\Lambda_{\rm QCD} = 0.226$ GeV. In [11], for pion PDF evolution, the initial scale in leading order evolution was found to be $\mu_0 = 0.313$ GeV. For protons, we use the same initial scale.

The LFWFs are independent of the hard evolution scale μ. Generally, the models of LFWFs are defined at the

lowest scale [4] and then the Dokshitzer-Gribov-Lipatov-Altarelli-Parisi equation determines the PDF scale evolution. Thus, in the LFWF overlap representation, the unpolarized PDFs in the light front diquark model at the initial scale μ_0 are obtained as

$$f_1^{(S)}(x) = \int d^2\mathbf{p}_\perp \frac{1}{16\pi^3}[|\psi_+^{+(u)}(x,\mathbf{p}_\perp)|^2 + |\psi_-^{+(u)}(x,\mathbf{p}_\perp)|^2],$$
$$= N_S^2\left[\frac{1}{\delta^u}x^{2a_1^u}(1-x)^{2b_1^u+1} + x^{2a_2^u-2}(1-x)^{2b_2^u+3}\frac{\kappa^2}{(\delta^u)^2M^2\ln(1/x)}\right], \quad (40)$$

for the scalar diquark, and

$$f_1^{(A)}(x) = \int d^2\mathbf{p}_\perp \frac{1}{16\pi^3}[|\psi_{++}^{+(\nu)}(x,\mathbf{p}_\perp)|^2 + |\psi_{-+}^{+(\nu)}(x,\mathbf{p}_\perp)|^2 + |\psi_{+0}^{+(\nu)}(x,\mathbf{p}_\perp)|^2 + |\psi_{-0}^{+(\nu)}(x,\mathbf{p}_\perp)|^2]$$
$$= \left(\frac{1}{3}N_0^{(\nu)2} + \frac{2}{3}N_1^{(\nu)2}\right) \times \left[\frac{1}{\delta^\nu}x^{2a_1^\nu}(1-x)^{2b_1^\nu+1} + x^{2a_2^\nu-2}(1-x)^{2b_2^\nu+3}\frac{\kappa^2}{(\delta^\nu)^2M^2\ln(1/x)}\right] \quad (41)$$

for the vector diquark, where A represents the isoscalar-vector (V) diquark corresponding to the u quark and the isovector-vector (VV) diquark corresponding to the d quark.

We simulate the scale evolution of the PDF by making the parameters in the PDF scale dependent, such that the values of the parameters at μ_0 are the same as in the LFWFs. Thus, at a scale μ, we parametrize the expressions for the PDFs as

$$f_1^{(S)}(x,\mu) = N_S^2(\mu)\left[\frac{1}{\delta^u(\mu)}x^{2a_1^u(\mu)}(1-x)^{2b_1^u(\mu)+1} + x^{2a_2^u(\mu)-2}(1-x)^{2b_2^u(\mu)+3}\frac{\kappa^2}{(\delta^u(\mu))^2M^2\ln(1/x)}\right], \quad (42)$$

$$f_1^{(A)}(x,\mu) = \left(\frac{1}{3}N_0^{(\nu)2}(\mu) + \frac{2}{3}N_1^{(\nu)2}(\mu)\right) \times \left[\frac{1}{\delta^\nu(\mu)}x^{2a_1^\nu(\mu)}(1-x)^{2b_1^\nu(\mu)+1} + x^{2a_2^\nu(\mu)-2}(1-x)^{2b_2^\nu(\mu)+3}\frac{\kappa^2}{(\delta^\nu(\mu))^2M^2\ln(1/x)}\right]. \quad (43)$$

The assumption is that, not only does a set of parameters exist at every scale to reproduce the desired PDFs but we can also define an evolution formula for each of these parameters consistent with PDF evolution, starting from the initial scale μ_0.

The flavor decomposed PDFs are given as, from Eqs. (10)–(11),

$$f_1^u(x,\mu) = C_S^2 f_1^{(S)}(x,\mu) + C_V^2 f_1^{(V)}(x,\mu), \quad (44)$$

$$f_1^d(x,\mu) = C_{VV}^2 f_1^{(VV)}(x,\mu). \quad (45)$$

The PDF $f_1^\nu(x,\mu)$ at a scale μ can be written in our model as

$$f_1^\nu(x,\mu) = N^{(\nu)}(\mu)\left[\frac{1}{\delta^\nu(\mu)}x^{2a_1^\nu(\mu)}(1-x)^{2b_1^\nu(\mu)+1} + x^{2a_2^\nu(\mu)-2}(1-x)^{2b_2^\nu(\mu)+3}\frac{\kappa^2}{(\delta^\nu(\mu))^2M^2\ln(1/x)}\right]. \quad (46)$$

The evolution of the parameters should be such that the PDF satisfies the master evolution equation, Eq. (37). The overall constants $N^{(u)}(\mu) = (C_S^2 N_s^2(\mu) + C_V^2(\frac{1}{3}N_0^{(u)2}(\mu) + \frac{2}{3}N_1^{(u)2}(\mu)))$ and $N^{(d)}(\mu) = C_{VV}^2(\frac{1}{3}N_0^{(d)2}(\mu) + \frac{2}{3}N_1^{(d)2}(\mu))$ for u and d quarks, respectively. All the normalization constants at scale μ are determined by the normalization conditions defined in Eqs. ((27)–(30). To fit the PDF data from NNPDF21(NNLO) [48], we find that the scale dependence of the parameters can be written as

$$a_i^\nu(\mu) = a_i^\nu(\mu_0) + A_i^\nu(\mu), \quad (47)$$

$$b_i^\nu(\mu) = b_i^\nu(\mu_0) - B_i^\nu(\mu)\frac{4C_F}{\beta_0}\ln\left(\frac{\alpha_s(\mu^2)}{\alpha_s(\mu_0^2)}\right), \quad (48)$$

$$\delta^\nu(\mu) = \exp[\delta_1^\nu(\ln(\mu^2/\mu_0^2))^{\delta_2^\nu}], \quad (49)$$

where the $a_i^\nu(\mu_0)$ and $b_i^\nu(\mu_0)$ are the parameters at $\mu = \mu_0$, given in Table I. The parameter δ^ν becomes unity at μ_0 for both u and d quarks, as shown in Table I. The scale-dependent parts $A_i^\nu(\mu)$ and $B_i^\nu(\mu)$ evolve as

$$P_i^\nu(\mu) = \alpha_{P,i}^\nu \mu^{2\beta_{P,i}^\nu}\left[\ln\left(\frac{\mu^2}{\mu_0^2}\right)\right]^{\gamma_{P,i}^\nu}\Big|_{i=1,2}, \quad (50)$$

TABLE I. The fitted parameters for u and d quarks.

ν	a_1^ν	b_1^ν	a_2^ν	b_2^ν	δ^ν
u	0.280 ± 0.001	0.1716 ± 0.0051	0.84 ± 0.02	0.2284 ± 0.0035	1.0
d	0.5850 ± 0.0003	0.7000 ± 0.0002	$0.9434^{+0.0017}_{-0.0013}$	$0.64^{+0.0082}_{-0.0022}$	1.0

TABLE II. Electromagnetic radii of nucleon in this model compared with measured data [49].

Quantity	Our result	Measured data [49]
r_E^p (fm)	0.830 ± 0.025	0.877 ± 0.005
r_M^p (fm)	0.779 ± 0.007	0.777 ± 0.016
$\langle r_E^2 \rangle^n$ (fm^2)	-0.064 ± 0.018	-0.1161 ± 0.0022
r_M^n (fm)	0.758 ± 0.005	$0.862^{+0.009}_{-0.008}$

where the subscript P in the right-hand side of the above equation stands for $P = A$, B, corresponding to $P_i^\nu(\mu) = A_i^\nu(\mu), B_i^\nu(\mu)$, respectively. Note that at $\mu = \mu_0$, $P_i^\nu(\mu_0) = 0$. The unpolarized PDF data are fitted for $\mu^2 = 1$, 6, 16, 30, 65, and 150 GeV^2. The evolution parameters $\alpha_{P,i}^\nu, \beta_{P,i}^\nu$, and $\gamma_{P,i}^\nu$ are given in Table III and the δ_i^ν's are given in Table IV with the least χ^2 per degrees of freedom (χ^2/d.o.f.) corresponding to the PDF fit. The variation of $a_i^\nu(\mu)$, $b_i^\nu(\mu)$, and $\delta^\nu(\mu)$ with scale μ is shown in Figs. 5 and 6, respectively. At the initial scale μ_0, the strong coupling constant is large, $\alpha_s(\mu_0)/2\pi \sim 0.34$, and hence parameters evolve very fast for scales near the initial point. The rate of evolution decays down at higher scales where the coupling constant becomes small. In Appendix A, we have listed the parameters at different scales and shown the fitting of the parameters at the above-mentioned scales.

With the fitted parameters, we predict the unpolarized PDF at other scales and compare with NNPDF21(NNLO), HERAPDF15(NNLO), and MSTW2008(NNLO) results in Fig. 7. Although, to determine the evolution, we used up to $\mu^2 = 150$ GeV^2, Fig. 7 shows that the model reproduces the PDF quite accurately at very high scales. According to the Drell-Yan-West relation [50,51], the quark distribution should go like $(1-x)^p$ as $x \to 1$ at large μ^2 and the Dirac form factor $F_1(Q^2) \sim 1/(Q^2)^{(p+1)/2}$ as $Q^2 \to \infty$, where p is related to the number of valence quarks. For, protons, the number of valence quarks is three, which also gives $p = 3$. In our model, we observe that for u-quarks the unpolarized PDF at large μ^2 goes as $f_1^u \sim (1-x)^{3.35}$ as $x \to 1$ [for d quarks, $f_1^d \sim (1-x)^{3.09}$], and $F_1(Q^2) \sim 1/(Q^2)^{2.16}$ at large Q^2, which are consistent with the Drell-Yan-West relation.

TABLE IV. PDF evolution parameter δ_1^ν and δ_2^ν for $\nu = u$, d.

$\delta^\nu(\mu)$	δ_1^ν	δ_2^ν	χ^2/d.o.f.
δ^u	0.015 ± 0.008	1.667 ± 0.032	1.16
δ^d	0.212 ± 0.0566	0.5444 ± 0.1504	0.81

With these above PDF evolution parameters we can generate the scale evolution of the other distribution functions, e.g., helicity distribution, transversity distribution, GPDs, TMDs, etc. Now we show that the model can predict the helicity and transversity distributions at different scales.

V. MODEL PREDICTIONS

A. Helicity distributions and axial charges

The polarized PDFs are evaluated as predictions of the model. In terms of the light front wave functions, the helicity distribution $g_1(x)$ in the quark-diquark model at the initial scale μ_0 is defined as

$$g_1^{(S)}(x) = \int d^2\mathbf{p}_\perp \frac{1}{16\pi^3}[|\psi_+^{+(u)}(x,\mathbf{p}_\perp)|^2 - |\psi_-^{+(u)}(x,\mathbf{p}_\perp)|^2], \tag{51}$$

$$g_1^{(A)}(x) = \int d^2\mathbf{p}_\perp \frac{1}{16\pi^3}[|\psi_{++}^{+(\nu)}(x,\mathbf{p}_\perp)|^2 - |\psi_{-+}^{+(\nu)}(x,\mathbf{p}_\perp)|^2 + |\psi_{+0}^{+(\nu)}(x,\mathbf{p}_\perp)|^2 - |\psi_{-0}^{+(\nu)}(x,\mathbf{p}_\perp)|^2], \tag{52}$$

for scalar and vector diquarks, respectively. The scale evolutions of the polarized PDFs are simulated by the same scheme as the unpolarized PDF. The scale evolutions of the parameters are the same as given in Eqs. (47)–(50). Thus, the flavor-dependent helicity distributions at a scale μ are given by

TABLE III. PDF evolution parameters with 95% confidence bounds.

$P_i^\nu(\mu)$	α_i^ν	β_i^ν	γ_i^ν	χ^2/d.o.f.
A_1^u	-0.2058 ± 0.0187	-0.0318 ± 0.0209	0.405 ± 0.0937	0.23
B_1^u	$1.551^{+0.034}_{-0.035}$	0.0598 ± 0.0057	-0.4291 ± 0.0242	0.02
A_2^u	-0.1637 ± 0.0179	-0.0066 ± 0.0245	0.3758 ± 0.1111	0.13
B_2^u	1.426 ± 0.320	0.07780.0605	$-0.7634^{+0.0241}_{-0.0251}$	0.07
A_1^d	0.0061 ± 0.0098	-0.1535 ± 0.0257	$1.391^{+0.246}_{-0.245}$	0.14
B_1^d	2.072 ± 0.0193	$-0.008^{+0.021}_{-0.022}$	0.1728 ± 0.0972	0.10
A_2^d	-0.2493 ± 0.0456	-0.0116 ± 0.0408	0.1371 ± 0.1783	0.29
B_2^d	0.1399 ± 0.0737	0.0247 ± 0.1086	$0.5733^{+0.0517}_{-0.0518}$	0.10

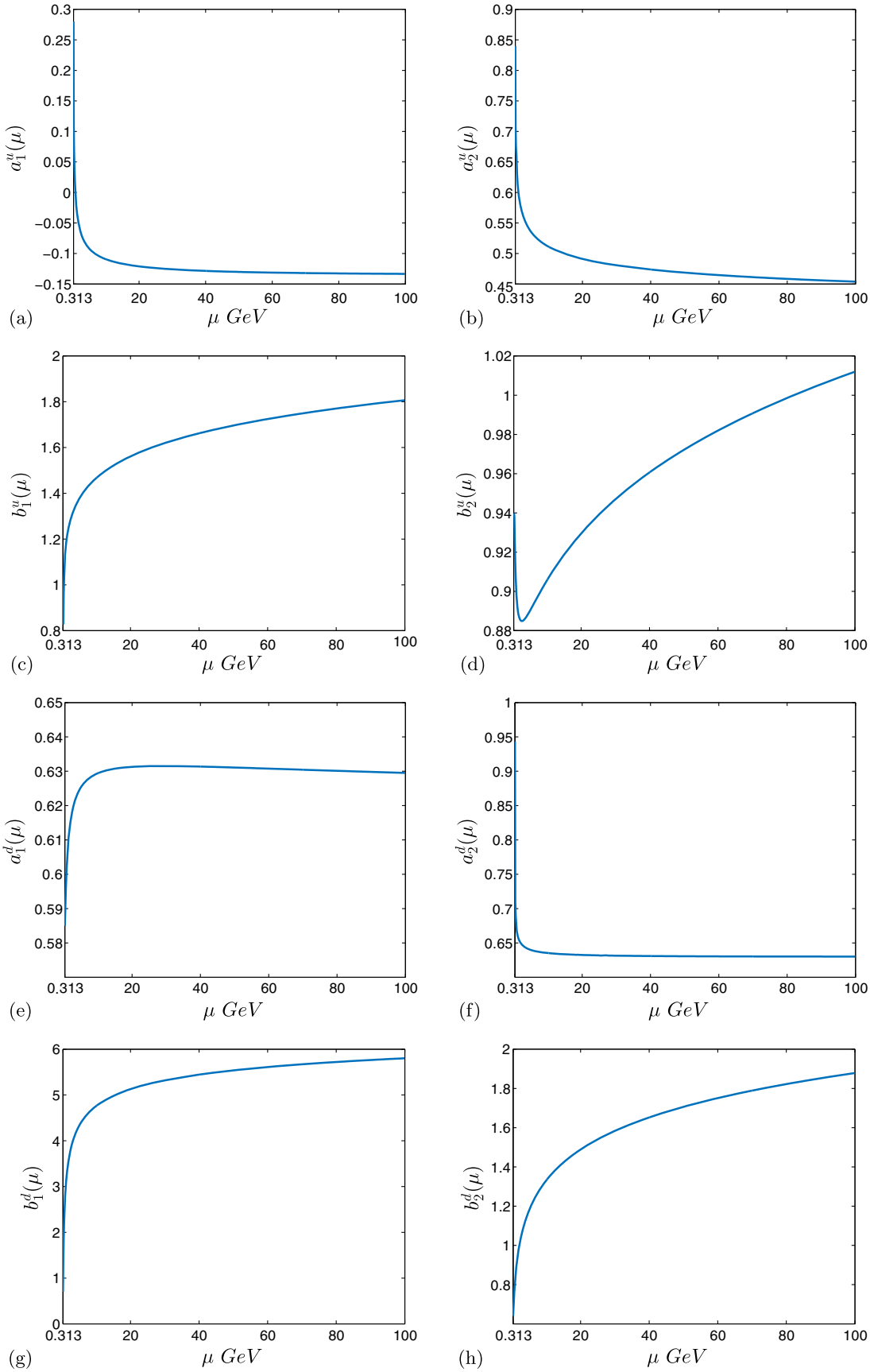

FIG. 5. Scale evolution of the parameters [Eqs. (47)–(48)].

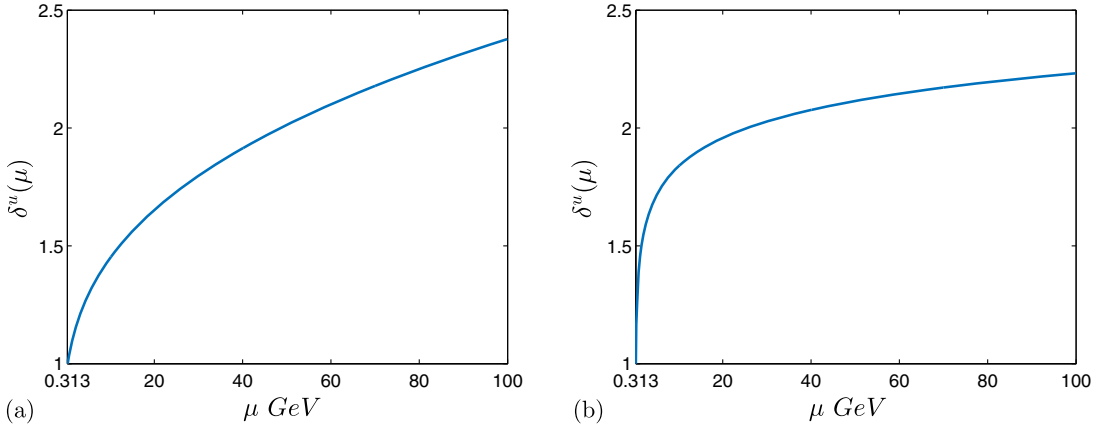

FIG. 6. Variation of δ^v with μ for the u and d quark; see Eq. (49).

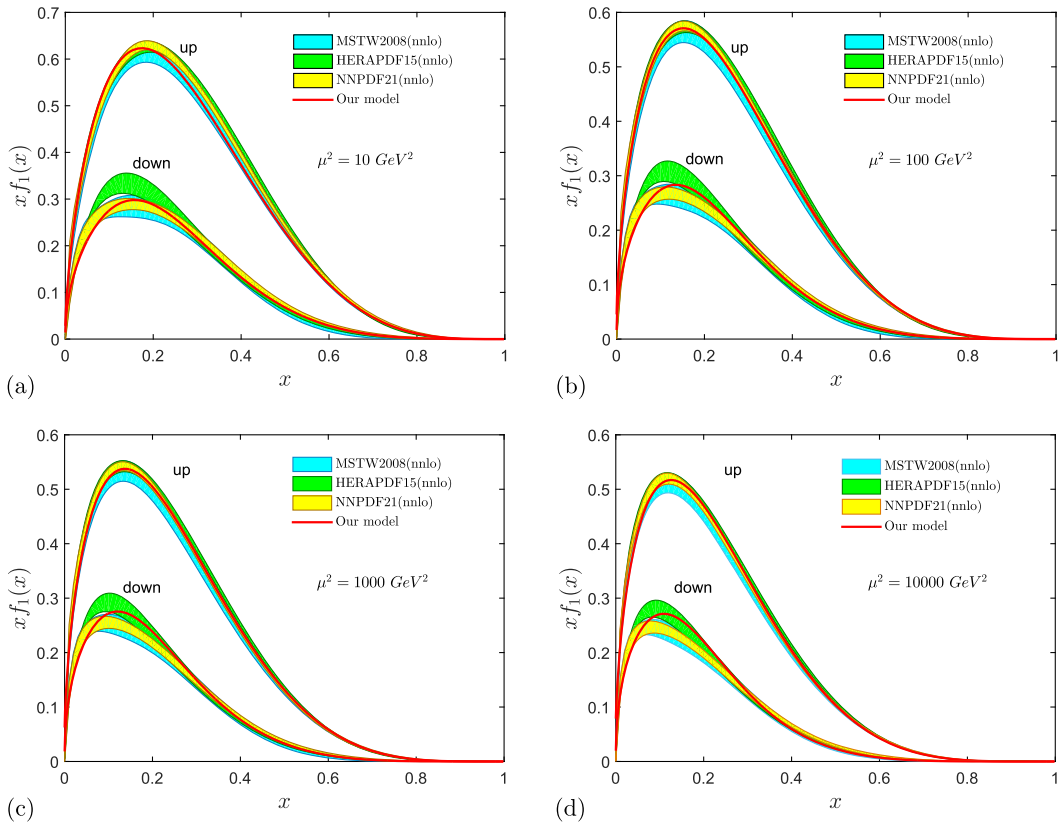

FIG. 7. Evolution of unpolarized PDFs in this model at $\mu^2 = 10$, 100, 1000, and 10000 GeV^2 for both u and d quarks. Our model predictions are compared with NNPDF21(NNLO) [48], HERAPDF15(NNLO) [52] and MSTW2008(NNLO) [53] results.

$$g_1^u(x,\mu) = \left(C_S^2 N_S^2(\mu) + C_V^2\left(\frac{1}{3}N_0^{(u)2}(\mu) - \frac{2}{3}N_1^{(u)2}(\mu)\right)\right) \times \left[\frac{1}{\delta^u(\mu)}x^{2a_1^u(\mu)}(1-x)^{2b_1^u(\mu)+1} - x^{2a_2^u(\mu)-2}(1-x)^{2b_2^u(\mu)+3}\frac{\kappa^2}{(\delta^u(\mu))^2 M^2 \ln(1/x)}\right], \tag{53}$$

$$g_1^d(x,\mu) = C_{VV}^2\left(\frac{1}{3}N_0^{(d)2}(\mu) - \frac{2}{3}N_1^{(d)2}(\mu)\right) \times \left[\frac{1}{\delta^d(\mu)}x^{2a_1^d(\mu)}(1-x)^{2b_1^d(\mu)+1} - x^{2a_2^d(\mu)-2}(1-x)^{2b_2^d(\mu)+3}\frac{\kappa^2}{(\delta^d(\mu))^2 M^2 \ln(1/x)}\right]. \tag{54}$$

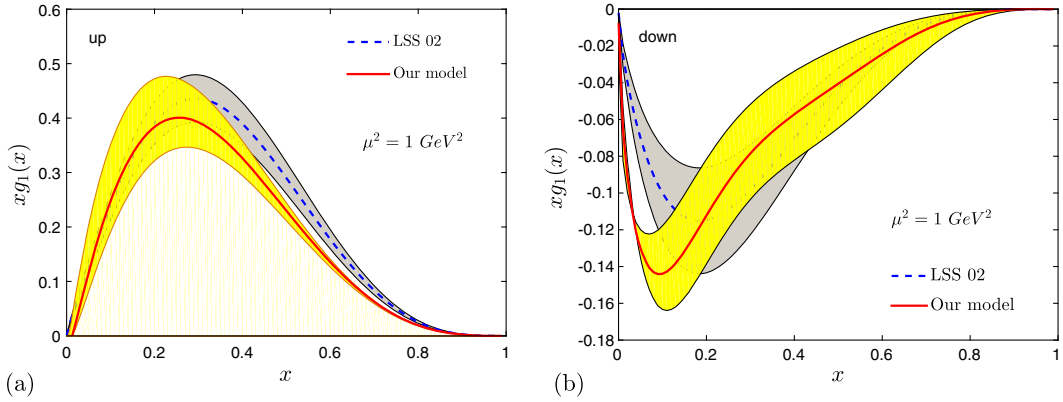

FIG. 8. Helicity PDF at $\mu^2 = 1$ GeV^2 compared with Ref. [55]. The (yellow) error bands in our model come from the errors in the evolution parameters given in Table III.

Helicity PDFs $g_1(x)$ are shown in Fig. 8, at scale $\mu^2 = 1$ GeV^2, for u and d quarks. Following [4,54], we include a constant relative error of 10% to g_1^u and 25% to g_1^d in the data taken from [55]. The errors in the model predictions are due to the uncertainties in the parameters as listed in Table V. The model predicts the helicity PDF for u quarks quite well.

The axial charges that are obtained from the first moment of the helicity distributions are given in Table V and compared with the measured data [56]. The axial charge of the proton is defined as

$$g_A = g_A^u - g_A^d. \tag{55}$$

The model prediction is in excellent agreement with the experimental data. The second moments of the helicity distributions are also presented in the table, where $g_A^{\nu(1)} = \int_0^1 dx x g_1^\nu(x)$ and $g_A^{(1)}$ is defined as

$$g_A^{(1)} = \int_0^1 dx x(g_1^u(x) - g_1^d(x)). \tag{56}$$

In Fig. 9(a), the scale evolution of the axial charges for u and d quarks are shown. The top panels in Fig. 9(a) represent the axial charge of the proton, g_A. Results from other models and experimental data are shown in the same plot for comparison. Results from other models, e.g., NQM, LFCQM, and LFχQSM [57] at $\mu^2 = 0.26$ GeV^2 are in agreement with our model prediction, and again our model predicts the experimental data at $\mu^2 = 1$ GeV^2 (shown in red in Fig. 9) quite well. In Fig. 9(b), the scale evolution of the second moment of the helicity distributions for both u and d quarks are shown and compared with other model predictions and experimental data. The top panel in the plot represents $g_A^{(1)}$. Our model predictions show excellent agreement with the experimental data available at $\mu^2 = 1$ GeV^2.

B. Transversity distributions and tensor charges

The transversity distributions in this model read

$$h_1^u(x,\mu) = \left(C_S^2 N_S^2(\mu) - C_V^2 \frac{1}{3} N_0^{(u)2}(\mu)\right) \frac{1}{\delta^u} x^{2a_1^u(\mu)}(1-x)^{2b_1^u(\mu)+1}, \tag{57}$$

$$h_1^d(x,\mu) = -C_{VV}^2 \frac{1}{3} N_0^{(d)2}(\mu) \frac{1}{\delta^d} x^{2a_1^d(\mu)}(1-x)^{2b_1^d(\mu)+1}. \tag{58}$$

Transversity PDFs $h_1(x)$ are shown in Fig. 10, at scale $\mu^2 = 1$ GeV^2, for u and d quarks. The model predictions are shown to agree with the experimental data [58]. The first moment of the transversity distribution gives the tensor charge g_T. The model again predicts the tensor charges quite accurately as shown in Table VI. For both u and d quarks, we have $|g_T^\nu| < |g_A^\nu|$. In Fig. 11(a), we have compared our model predictions of the tensor charge for both u and d quarks with other models along with the phenomenological fit of experimental data [58]. Similar comparisons are given in studies by Anselmino *et al.* [58]

TABLE V. Axial charge and second moment of helicity distribution at the scale $\mu^2 = 1$ GeV^2 and compared with the Leader-Sidorov-Stamenov fit to experimental data [56].

	g_A^u	g_A^d	g_A	$g_A^{u(1)}$	$g_A^{d(1)}$	$g_A^{(1)}$
Our result	0.71 ± 0.09	$-0.54^{+0.19}_{-0.13}$	$1.25^{+0.28}_{-0.22}$	0.18 ± 0.15	$-0.052^{+0.003}_{-0.007}$	$0.23^{+0.15}_{-0.16}$
Measured data [56]	0.82 ± 0.07	-0.45 ± 0.07	1.27 ± 0.14	0.19 ± 0.07	-0.06 ± 0.07	0.25 ± 0.14

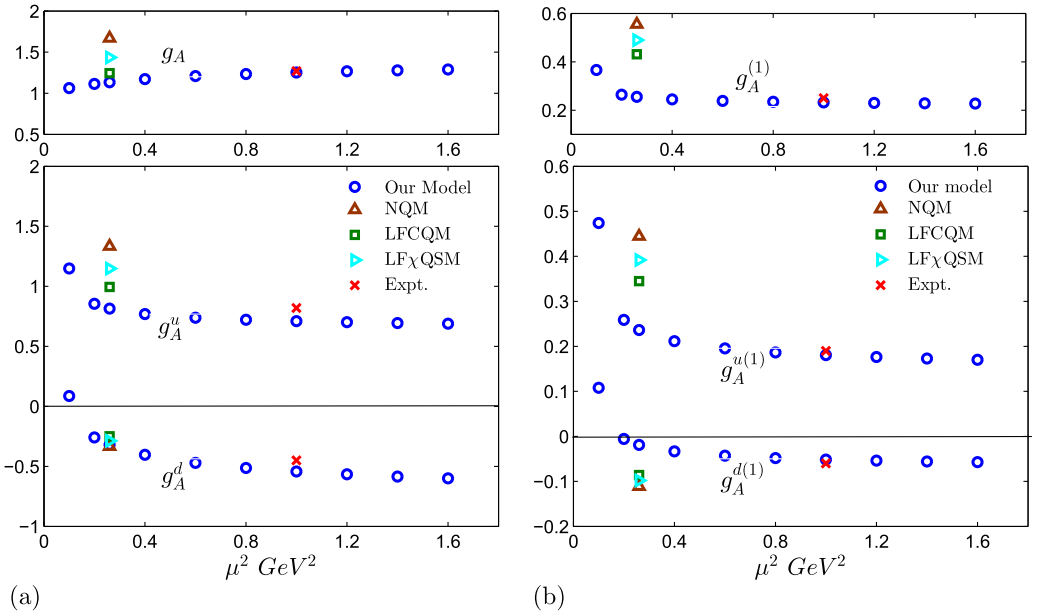

FIG. 9. (a) Scale evolution of axial charge in the range $\mu^2 = 0.1$ to 1.6 GeV^2. We compare our result with other models, e.g., NQM, LFCQM, LFχQSM [57] for $\mu^2 = 0.26$ GeV^2 and also with the experimental value at $\mu^2 = 1.0$ GeV^2 [56]. (b) The second moment of helicity and a comparison with measured value [56] at $\mu^2 = 0.26$, 1.0 GeV^2. The top panels in the plots represent (a) the total proton axial charge and (b) the second moment of the total helicity distribution.

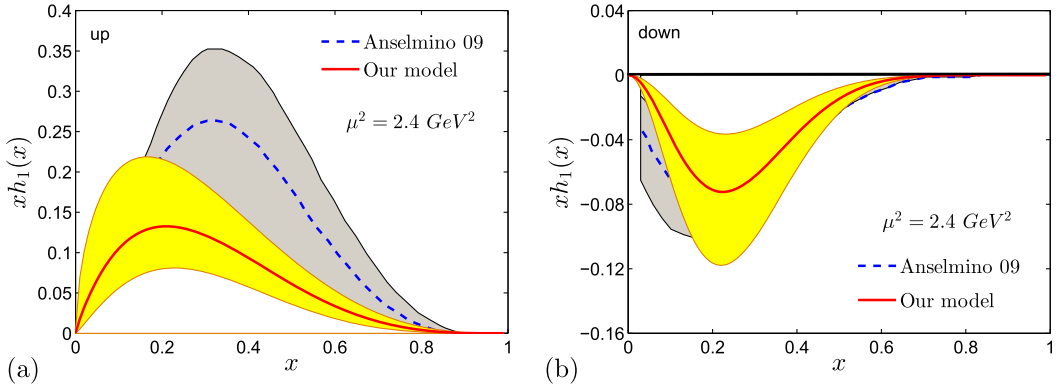

FIG. 10. The transversity distribution at $\mu^2 = 2.4$ GeV^2 for (a) u quarks and (b) d quarks. Our results are compared with Anselmino *et al.* [58].

and Wakamatsu [59]. Our predictions fall within the uncertainty bands of the phenomenological fits for both u and d quarks. The ratio of the two tensor charges $|g_T^d/g_T^u|$ is totally scale independent and a better quantity to compare with other models. Figure 11(b) shows the comparison of that ratio with other model predictions. Our model predicts $|g_T^d/g_T^u| = 0.38$, which is very close to the phenomenological prediction.

TABLE VI. Tensor charge at the scale $\mu^2 = 0.8$ GeV^2. Our results are compared with measured data [64].

	g_T^u	g_T^d	g_T
Our result	$0.37^{+0.06}_{-0.05}$	$-0.14^{+0.05}_{-0.06}$	$0.51^{+0.12}_{-0.11}$
Measured data [64]	$0.59^{+0.14}_{-0.13}$	$-0.20^{+0.05}_{-0.07}$	$0.79^{+0.19}_{-0.20}$

This model also satisfies the Soffer bound, which at an arbitrary scale μ is defined as [65]

$$|h_1^\nu(x,\mu)| \le \frac{1}{2}[f_1^\nu(x,\mu) + g_1^\nu(x,\mu)]. \tag{59}$$

In Fig. 12 we show the lhs and rhs of the above equation multiplied by x for both $\nu = u$, d and at both low and high scales. According to the Soffer bound, the lhs should always lie below the rhs, which can be easily seen in Fig. 12.

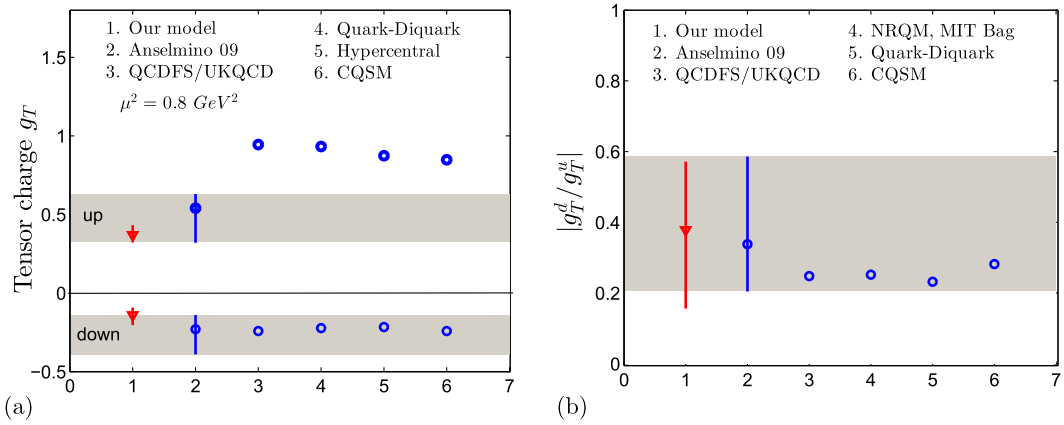

FIG. 11. (a) Comparisons of tensor charges gT with the experimental data fit [58] and other model predictions [60–63] for u and d quarks. The shaded regions are the error band for u and d quarks in the experimental extraction of g_T [58]. Our results of tensor charges for both u and d quarks are shown in red. (b) The ratio of the tensor charges $|g_T^d/g_T^u|$. Our results are compared with other models, e.g., lattice QCD [60], the MIT bag model, the quark-diquark model [61], and constituted quark soliton model (CQSM) [63].

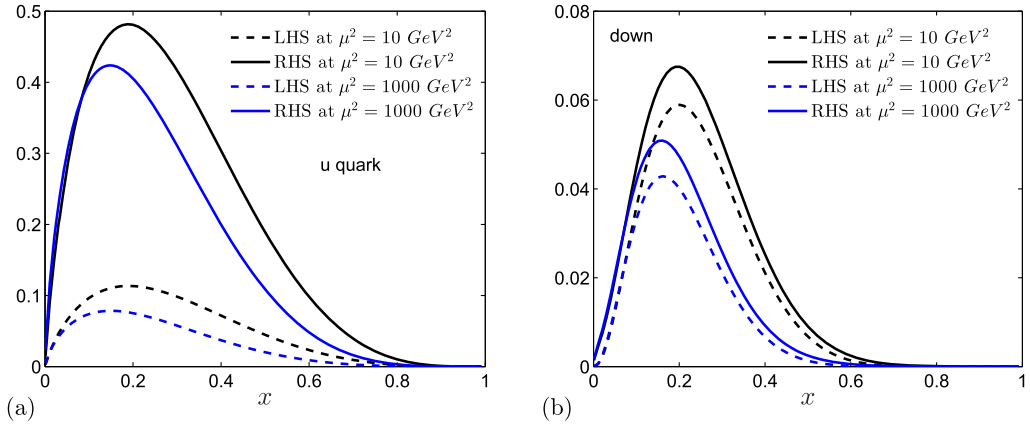

FIG. 12. The Soffer bound at $\mu^2 = 10$ GeV^2 and 1000 GeV^2 for (a) u quarks and (b) d quarks, where LHS and RHS stand for the left-hand side and right-hand side of Eq. (59) multiplied by x.

The proton momentum fraction carried by valence quarks can be estimated from the unpolarized PDFs at different scales μ:

$$P_q(\mu) = \int dx x[C_S^2 f_1^{(s)}(x) + C_V^2 f_1^{(V)}(x) + C_{VV}^2 f_1^{(VV)}(x)],$$
$$= \int dx x[f_1^{(u)}(x,\mu) + f_1^{(d)}(x,\mu)]. \quad (60)$$

The values of P_q with the scale are shown in Table VII. The momentum carried by the valence quarks decreases as the value of μ^2 increases.

TABLE VII. Proton momentum fraction carried by valence quarks P_q with the scale μ. The value given within square bracket is the ZEUS result [66] at the scale $\mu^2 = 7$ GeV^2.

μ^2 (GeV^2)	0.2	0.6	1.0	7.0	10	20
P_q	0.60	0.48	0.45	0.38[0.55]	0.37	0.35

VI. SUMMARY AND CONCLUSION

Light front AdS/QCD has predicted many interesting nucleon properties. Light front AdS/QCD predicts a particular form of wave function for a two-body bound state [5]. In this paper, we have developed a quark-diquark model for protons in which the light front wave functions are constructed from the AdS/QCD predictions. The model is consistent with the quark counting rule and Drell-Yan-West relation. The model has $SU(4)$ spin-flavor structure and includes the contributions from scalar ($S = 0$) and axial vector ($S = 1$) diquarks. The evolution of $f_1(x)$ is simulated by introducing scale-dependent parameters in the PDF. The scale evolutions of the parameters are determined by satisfying the PDF evolution in the range $\mu^2 =$ 0.09 GeV^2 to 150 GeV^2. We have given the explicit scale evolution of each parameter in the model, so the distributions can be calculated at any arbitrary scale. Though PDF data up to $\mu^2 = 150$ GeV^2 are used to determine the scale

evolution, we have shown that our model can accurately predict the PDF evolution up to a very high scale ($\mu^2 = 10^4$ GeV^2). The helicity and transversity PDFs are calculated as predictions of the model and are shown to satisfy the Soffer bound and have good agreement with the available data. Our model reproduces the experimental values of axial and tensor charges quite well. It will be interesting to study the other proton properties like GPDs, TMDs, Wigner distributions, GTMDs, etc., and their scale evolutions in this model, and to compare with other model predictions.

ACKNOWLEDGMENTS

D. C. thanks Stan Brodsky and Guy de Teramond for many insightful discussions. We also thank Chandan Mondal for many useful discussions.

APPENDIX: PARAMETER FITTING FOR PDF EVOLUTION

Scale evolutions of A_i^ν and B_i^ν are parametrized by the parameters $\alpha_i^\nu, \beta_i^\nu$, and γ_i^ν and that of δ^ν is parametrized by δ_1^ν and δ_2^ν. $f_1(x,\mu)$ is given by Eq. (46) along with Eqs. (47)–(49) and Eq. (50). Here we list the parameters A_i^ν, B_i^ν, and δ^ν fitted at different scales μ^2 in Tables VIII and IX. The last column in each table indicates the least χ^2 error in the PDF estimation. Each χ^2/d.o.f. has been evaluated from 100 data points for different $x(0 < x < 1)$; i.e., for the five-parameter fit, we have $100 - 5 = 95$ degrees of freedom. The fittings of the parameters at $\mu^2 = 1$, 6, 16, 30, 65, and 150 GeV^2 are shown in Figs. 13 and 14. The data points are extracted from the PDF data. The error bars shown in the plots are the errors in the extracted values of the parameters due to the uncertainties in the PDF data.

TABLE VIII. Fitting of the PDF $f_1(x)$ at various scales for u quarks.

μ^2 GeV^2	A_1^u	B_1^u	A_2^u	B_2^u	δ^u	χ^2/d.o.f.
1	-0.29 ± 0.009	1.08 ± 0.009	-0.225 ± 0.008	$0.75^{+0.047}_{-0.046}$	1.087 ± 0.029	1.41
6	-0.343 ± 0.003	0.94 ± 0.007	-0.275 ± 0.004	0.55 ± 0.013	1.176 ± 0.027	4.8
16	-0.365 ± 0.001	0.91 ± 0.007	$-0.295^{+0.003}_{-0.002}$	$0.52^{+0.013}_{-0.014}$	1.234 ± 0.014	1.8
30	-0.375 ± 0.004	$0.9^{+0.010}_{-0.012}$	$-0.31^{+0.003}_{-0.002}$	0.49 ± 0.005	1.298 ± 0.018	1.2
65	-0.386 ± 0.002	0.89 ± 0.004	$-0.323^{+0.002}_{-0.003}$	0.47 ± 0.009	1.389 ± 0.025	0.54
150	-0.392 ± 0.001	0.89 ± 0.002	$-0.334^{+0.0008}_{-0.001}$	0.46 ± 0.008	1.515 ± 0.034	0.29

TABLE IX. Fitting of the PDF $f_1(x)$ at various scales for d quarks.

μ^2 GeV^2	A_1^d	B_1^d	A_2^d	B_2^d	δ^d	χ^2/d.o.f.
1	0.02 ± 0.007	$2.4^{+0.029}_{-0.029}$	$-0.28^{+0.012}_{-0.017}$	$0.23^{+0.010}_{-0.011}$	1.43 ± 0.085	0.21
6	0.03 ± 0.007	$2.6^{+0.052}_{-0.051}$	$-0.29^{+0.006}_{-0.005}$	$0.32^{+0.024}_{-0.025}$	1.54 ± 0.065	0.38
16	0.036 ± 0.005	$2.68^{+0.017}_{-0.017}$	-0.298 ± 0.001	$0.38^{+0.009}_{-0.010}$	1.65 ± 0.044	0.40
30	0.042 ± 0.001	$2.74^{+0.018}_{-0.019}$	-0.305 ± 0.002	$0.42^{+0.008}_{-0.010}$	1.75 ± 0.030	0.49
65	0.044 ± 0.002	$2.78^{+0.020}_{-0.020}$	-0.308 ± 0.001	0.46 ± 0.010	1.82 ± 0.048	0.59
150	0.045 ± 0.001	$2.8^{+0.021}_{-0.020}$	-0.309 ± 0.0008	$0.49^{+0.016}_{-0.019}$	1.86 ± 0.036	0.77

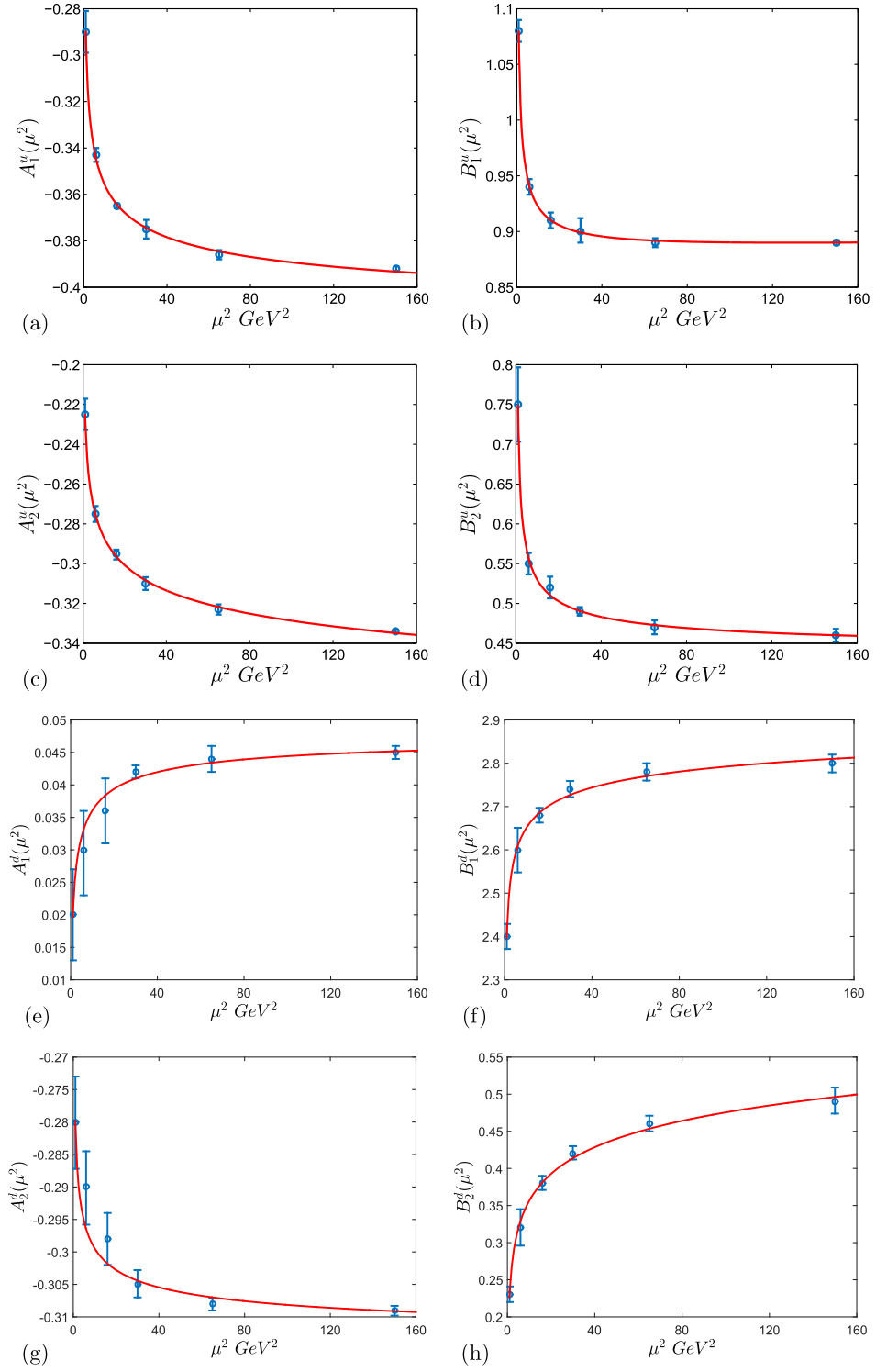

FIG. 13. Using Eq. (50), the data of Table VIII are fitted by varying evolution parameters $\alpha^{\nu}_{P,i}$, $\beta^{\nu}_{P,i}$, and $\gamma^{\nu}_{P,i}$, for u quarks [(a)–(d), respectively]. Similar data fitting plots for d quarks (Table IX) are shown in (e)–(h).

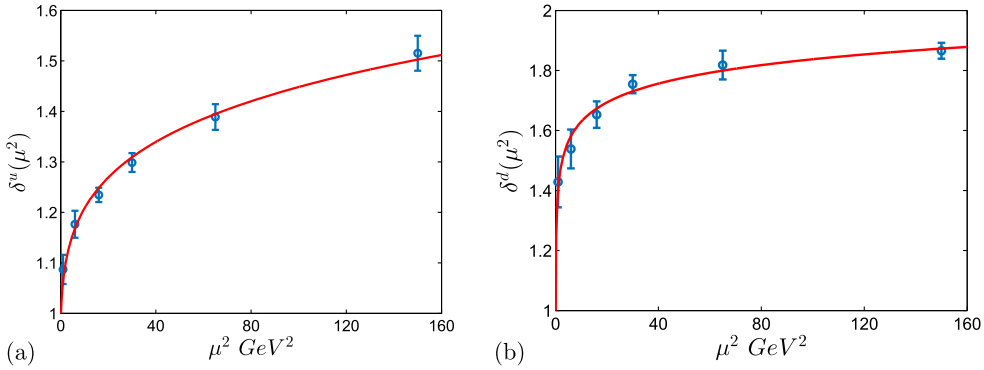

FIG. 14. The data of Table IV are fitted by varying evolution parameters δ_1^ν and δ_2^ν, for (a) u quark and (b) d quark.

[1] P. Kroll, M. Schurmann, and W. Schweiger, Electromagnetic form-factors of the nucleon in the few GeV region, Z. Phys. A **338**, 339 (1991); Exclusive photon-proton reactions at moderately large momentum transfer, Int. J. Mod. Phys. A **06**, 4107 (1991).

[2] R. Jakob, P. Kroll, M. Schurmann, and W. Schweiger, Octet baryon form-factors in the diquark model, Z. Phys. A **347**, 109 (1993).

[3] R. Jakob, P. J. Mulders, and J. Rodrigues, Modeling quark distribution and fragmentation functions, Nucl. Phys. **A626**, 937 (1997).

[4] A. Bacchetta, F. Conti, and M. Radici, Transverse-momentum distributions in a diquark spectator model, Phys. Rev. D **78**, 074010 (2008).

[5] S. J. Brodsky and G. F. de Teramond, Light-front dynamics and AdS/QCD correspondence: The pion form factor in the space- and time-like regions, Phys. Rev. D **77**, 056007 (2008); G. F. de Teramond and S. J. Brodsky, Hadronic form factor models and spectroscopy within the gauge/gravity correspondence, arXiv:1203.4025.

[6] T. Gutsche, V. E. Lyubovitskij, I. Schmidt, and A. Vega, Light-front quark model consistent with Drell-Yan-West duality and quark counting rules, Phys. Rev. D **89**, 054033 (2014); Erratum, Phys. Rev. D **92**, 019902(E) (2015).

[7] T. Gutsche, V. E. Lyubovitskij, I. Schmidt, and A. Vega, Nucleon structure in a light-front quark model consistent with quark counting rules and data, Phys. Rev. D **91**, 054028 (2015).

[8] C. Mondal and D. Chakrabarti, Generalized parton distributions and transverse densities in a light-front quark-diquark model for the nucleons, Eur. Phys. J. C **75**, 261 (2015); D. Chakrabarti and C. Mondal, Chiral-odd generalized parton distributions for proton in a light-front quark-diquark model, Phys. Rev. D **92**, 074012 (2015); D. Chakrabarti, C. Mondal, and A. Mukherjee, Gravitational form factors and transverse spin sum rule in a light front quark-diquark model in AdS/QCD, Phys. Rev. D **91**, 114026 (2015); D. Chakrabarti, T. Maji, C. Mondal, and A. Mukherjee, Wigner distributions and orbital angular momentum of a proton, Eur. Phys. J. C **76**, 409 (2016).

[9] A. Vega, I. Schmidt, T. Gutsche, and V. E. Lyubovitskij, Nucleon GPDs in a light-front quark model derived from soft-wall AdS/QCD, arXiv:1306.1597.

[10] T. Maji, C. Mondal, D. Chakrabarti, and O. V. Teryaev, Relating transverse structure of various parton distributions, J. High Energy Phys. 01 (2016) 165.

[11] W. Broniowski, E. Ruiz Arriola, and K. Golec-Biernat, Generalized parton distributions of the pion in chiral quark models and their QCD evolution, Phys. Rev. D **77**, 034023 (2008).

[12] G. P. Lepage and S. J. Brodsky, Exclusive processes in perturbative quantum chromodynamics, Phys. Rev. D **22**, 2157 (1980).

[13] J. R. Ellis, D. S. Hwang, and A. Kotzinian, Sivers asymmetries for inclusive pion and kaon production in deep-inelastic scattering, Phys. Rev. D **80**, 074033 (2009).

[14] D. Chakrabarti and C. Mondal, Generalized parton distributions for the proton in AdS/QCD, Phys. Rev. D **88**, 073006 (2013); Nucleon and flavor form factors in a light front quark model in AdS/QCD, Eur. Phys. J. C **73**, 2671 (2013).

[15] S. J. Brodsky and S. D. Drell, The anomalous magnetic moment and limits on fermion substructure, Phys. Rev. D **22**, 2236 (1980).

[16] G. D. Cates, C. W. de Jager, S. Riordan, and B. Wojtsekhowski, Flavor Decomposition of the Elastic Nucleon Electromagnetic Form Factors, Phys. Rev. Lett. **106**, 252003 (2011).

[17] M. Diehl and P. Kroll, Nucleon form factors, generalized parton distributions and quark angular momentum, Eur. Phys. J. C **73**, 2397 (2013).

[18] V. Punjabi *et al.*, Proton elastic form-factor ratios to $Q^2 = 3.5$ GeV^2 by polarization transfer, Phys. Rev. C **71**, 055202 (2005); Publisher's Note, Phys. Rev. C **71**, 069902(E) (2005).

[19] R. Pohl *et al.*, The size of the proton, Nature (London) **466**, 213 (2010); A. Antognini *et al.*, Proton structure from the

measurement of $2S-2P$ transition frequencies of muonic hydrogen, Science **339**, 417 (2013).
[20] O. Gayou *et al.*, Measurements of the elastic electromagnetic form-factor ratio mu(p) G(Ep)/G(Mp) via polarization transfer, Phys. Rev. C **64**, 038202 (2001).
[21] M. K. Jones *et al.* (Jefferson Lab Hall A Collaboration), G(E(p))/G(M(p)) Ratio by Polarization Transfer in Polarized $ep \to e$ Polarized p, Phys. Rev. Lett. **84**, 1398 (2000).
[22] J. Arrington, W. Melnitchouk, and J. A. Tjon, Global analysis of proton elastic form factor data with two-photon exchange corrections, Phys. Rev. C **76**, 035205 (2007).
[23] O. Gayou *et al.* (Jefferson Lab Hall A Collaboration), Measurement of G(Ep)/G(Mp) in Polarized $ep \to e$ Polarized-p to $Q^2 = 5.6$ GeV^2, Phys. Rev. Lett. **88**, 092301 (2002).
[24] T. Pospischil *et al.* (A1 Collaboration), Measurement of G(E(p))/G(M(p)) via polarization transfer at $Q^2 = 0.4\,\mathrm{GeV}/c^2$, Eur. Phys. J. A **12**, 125 (2001).
[25] B. D. Milbrath *et al.* (Bates FPP Collaboration), A Comparison of Polarization Observables in Electron Scattering from the Proton and Deuteron, Phys. Rev. Lett. **80**, 452 (1998); Erratum, Phys. Rev. Lett. **82**, 2221(E) (1999).
[26] E. Geis *et al.* (BLAST Collaboration), The Charge Form Factor of the Neutron at Low Momentum Transfer from the H-2-Polarized (e-Polarized, e-Prime n) p Reaction, Phys. Rev. Lett. **101**, 042501 (2008).
[27] G. Warren *et al.* (Jefferson Lab E93-026 Collaboration), Measurement of the Electric Form-Factor of the Neutron at $Q^2 = 0.5$ and 1.0 GeV$^2/c^2$, Phys. Rev. Lett. **92**, 042301 (2004).
[28] S. Riordan *et al.*, Measurements of the Electric Form Factor of the Neutron up to $Q^2 = 3.4$ GeV^2 Using the Reaction $^3\mathrm{He}(e,e'n)pp$, Phys. Rev. Lett. **105**, 262302 (2010).
[29] J. Bermuth *et al.*, The neutron charge form-factor and target analyzing powers from polarized-He-3 (polarized-e,e-prime n) scattering, Phys. Lett. B **564**, 199 (2003).
[30] B. Plaster *et al.* (Jefferson Laboratory E93-038 Collaboration), Measurements of the neutron electric to magnetic form-factor ratio G(En)/G(Mn) via the H-2(polarized-e, e-prime,polarized-n)H-1 reaction to $Q^2 = 1.45$ $(\mathrm{GeV}/c)^2$, Phys. Rev. C **73**, 025205 (2006).
[31] D. I. Glazier *et al.*, Measurement of the electric form-factor of the neutron at $Q^2 = 0.3$ $(\mathrm{GeV}/c)^2$ to 0.8 $(\mathrm{GeV}/c)^2$, Eur. Phys. J. A **24**, 101 (2005).
[32] R. Schiavilla and I. Sick, Neutron charge form-factor at large q^2, Phys. Rev. C **64**, 041002 (2001).
[33] J. Arrington, Extraction of two-photon contributions to the proton form-factors, Phys. Rev. C **71**, 015202 (2005).
[34] J. Lachniet *et al.* (CLAS Collaboration), A Precise Measurement of the Neutron Magnetic Form Factor $G^n(M)$ in the Few-GeV^2 Region, Phys. Rev. Lett. **102**, 192001 (2009).
[35] B. Anderson *et al.* (Jefferson Lab E95-001 Collaboration), Extraction of the neutron magnetic form-factor from quasi-elastic polarized-He-3 (polarized-e, e-prime) at $Q^2 = 0.1$–0.6 $(\mathrm{GeV}/c)^2$, Phys. Rev. C **75**, 034003 (2007).
[36] W. Xu *et al.* (Jefferson Lab E95-001 Collaboration), PWIA extraction of the neutron magnetic form-factor from quasielastic polarized-He-3 (polarized-e, e-prime) at $Q^2 = 0.3$ $(\mathrm{GeV}/c)^2$ to 0.6 $(\mathrm{GeV}/c)^2$, Phys. Rev. C **67**, 012201 (2003).
[37] G. Kubon *et al.*, Precise neutron magnetic form-factors, Phys. Lett. B **524**, 26 (2002).
[38] H. Anklin *et al.*, Precise measurements of the neutron magnetic form-factor, Phys. Lett. B **428**, 248 (1998).
[39] G. Ron *et al.* (Jefferson Lab Hall A Collaboration), Low Q^2 measurements of the proton form factor ratio mu_pG_E/G_M, Phys. Rev. C **84**, 055204 (2011).
[40] R. C. Walker *et al.*, Measurements of the proton elastic form-factors for $1 \le Q^2 \le 3(\mathrm{GeV}/C)^2$ at SLAC, Phys. Rev. D **49**, 5671 (1994).
[41] X. Zhan *et al.*, High-precision measurement of the proton elastic form factor ratio μ_pG_E/G_M at low Q^2, Phys. Lett. B **705**, 59 (2011).
[42] G. MacLachlan *et al.*, The ratio of proton electromagnetic form factors via recoil polarimetry at $Q^2 = 1.13$ $(\mathrm{GeV}/c)^2$, Nucl. Phys. **A764**, 261 (2006).
[43] M. Paolone *et al.*, Polarization Transfer in the 4He(e,e'p)3H Reaction at $Q^2 = 0.8$ and 1.3 $(\mathrm{GeV}/c)^2$, Phys. Rev. Lett. **105**, 072001 (2010).
[44] I. Passchier *et al.*, The Charge Form-Factor of the Neutron from the Reaction Polarized H-2 (polarized e, e-prime n) p, Phys. Rev. Lett. **82**, 4988 (1999).
[45] H. Zhu *et al.* (E93026 Collaboration), A Measurement of the Electric Form-Factor of the Neutron through Polarized-d (Polarized-e, e-Prime n)p at $Q^2 = 0.5$ $(\mathrm{GeV}/c)^2$, Phys. Rev. Lett. **87**, 081801 (2001).
[46] C. Herberg *et al.*, Determination of the neutron electric form-factor in the D(e,e' n)p reaction and the influence of nuclear binding, Eur. Phys. J. A **5**, 131 (1999).
[47] S. Riordan *et al.*, Measurements of the Electric Form Factor of the Neutron up to $Q^2 = 3.4$ GeV^2 using the Reaction $^3\mathrm{He}(e,e'n)pp$, Phys. Rev. Lett. **105**, 262302 (2010).
[48] L. Del Debbio *et al.* (NNPDF Collaboration), Neural network determination of parton distributions: The nonsinglet case, J. High Energy Phys. 03 (2007) 039.
[49] J. Beringer *et al.* (Particle Data Group Collaboration), Review of particle physics (RPP), Phys. Rev. D **86**, 010001 (2012).
[50] S. D. Drell and T. M. Yan, Connection of Elastic Electromagnetic Nucleon Form-Factors at Large Q^2 and Deep Inelastic Structure Functions Near Threshold, Phys. Rev. Lett. **24**, 181 (1970).
[51] G. B. West, Phenomenological Model for the Electromagnetic Structure of the Proton, Phys. Rev. Lett. **24**, 1206 (1970).
[52] F. D. Aaron *et al.* (H1 and ZEUS Collaborations), Combined measurement and QCD analysis of the inclusive e + − p scattering cross sections at HERA, J. High Energy Phys. 01 (2010) 109.
[53] A. D. Martin, W. J. Stirling, R. S. Thorne, and G. Watt, Parton distributions for the LHC, Eur. Phys. J. C **63**, 189 (2009).
[54] M. Hirai, S. Kumano, and N. Saito (Asymmetry Analysis Collaboration), Determination of polarized parton distribution functions and their uncertainties, Phys. Rev. D **69**, 054021 (2004).
[55] E. Leader and D. B. Stamenov, Can the polarization of the strange quarks in the proton be positive?, Phys. Rev. D **67**, 037503 (2003).
[56] E. Leader, A. V. Sidorov, and D. B. Stamenov, Determination of polarized PDFs from a QCD analysis of inclusive

and semi-inclusive deep inelastic scattering data, Phys. Rev. D **82**, 114018 (2010).

[57] C. Lorce, B. Pasquini, and M. Vanderhaeghen, Unified framework for generalized and transverse-momentum dependent parton distributions within a 3Q light-cone picture of the nucleon, J. High Energy Phys. 05 (2011) 041.

[58] M. Anselmino, M. Boglione, U. D'Alesio, A. Kotzinian, F. Murgia, A. Prokudin, and S. Melis, Update on transversity and Collins functions from SIDIS and e + e− data, Nucl. Phys. B, Proc. Suppl. **191**, 98 (2009).

[59] M. Wakamatsu, Chiral-odd GPDs, transversity decomposition of angular momentum, and tensor charges of the nucleon, Phys. Rev. D **79**, 014033 (2009).

[60] M. Gockeler, Ph. Hägler, R. Horsley, D. Pleiter, P.E.L. Rakow, A. Schäfer, G. Schierholz, and J. M. Zanotti (QCDSF and UKQCD Collaborations), Quark helicity flip generalized parton distributions from two-flavor lattice QCD, Phys. Lett. B **627**, 113 (2005).

[61] I. C. Cloet, W. Bentz, and A. W. Thomas, Transversity quark distributions in a covariant quark-diquark model, Phys. Lett. B **659**, 214 (2008).

[62] B. Pasquini, M. Pincetti, and S. Boffi, Chiral-odd generalized parton distributions in constituent quark models, Phys. Rev. D **72**, 094029 (2005).

[63] M. Wakamatsu, Comparative analysis of the transversities and the longitudinally polarized distribution functions of the nucleon, Phys. Lett. B **653**, 398 (2007).

[64] M. Anselmino, M. Boglione, U. D'Alesio, A. Kotzinian, F. Murgia, A. Prokudin, and C. Turk, Transversity and Collins functions from SIDIS and e + e− data, Phys. Rev. D **75**, 054032 (2007).

[65] J. Soffer, Positivity Constraints for Spin Dependent Parton Distributions, Phys. Rev. Lett. **74**, 1292 (1995).

[66] S. Chekanov *et al.* (ZEUS Collaboration), A ZEUS next-to-leading-order QCD analysis of data on deep inelastic scattering, Phys. Rev. D **67**, 012007 (2003).